Heliyon 10 (2024) e29453

Contents lists available at ScienceDirect

Heliyon

journal homepage: www.cell.com/heliyon

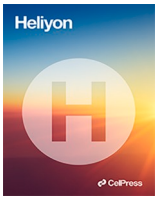

Research article

Effect of structural support size and position on depressed tibial plateau fractures: A finite element analysis

Xiaomeng Ren [a,1], Cheng Xu [a,1], Yu Jiang [a,1], Da Teng [b], Xinmo Liu [b], Junsong Wang [a], Wei Zhang [a,*]

[a] Senior Department of Orthopedics, The Fourth Medical Center of PLA General Hospital, 51 Fucheng Road, Haidian District, Beijing, 100089, China
[b] Senior Department of General Surgery, The First Medical Center of Chinese PLA General Hospital, 28 Fuxing Road, Haidian District, Beijing, 100089, China

ARTICLE INFO

Keywords:
Depressed tibial plateau fracture
Internal fixation
Structural support
Bone graft
Finite element analysis

ABSTRACT

Objective: Structural support for depressed tibial plateau fractures is receiving increasing attention. Currently, there has been little biomechanical evaluation of structural support. This work aimed to investigate the effect of structural support size and position on fracture fixation stability.
Methods: A split-depressed tibial plateau fracture model was created according to the fracture map. Cortical screws combined with structural filler were used for fracture fixation. The filler diameter was set to small, medium and large, and the filler position was set to the center and offset by 1, 2 and 3 mm to study the effect of position and size on stability.
Results: The maximum stress on the implant in all scenarios occurs at the lower contact surface between the anterior screw and the filler. Increased support size resulted in increased mean maximum screw stress, depressed fragment axial displacement and separated fragment transverse displacement (screw stress: 266.6 ± 37.7 MPa vs. 266.7 ± 51.0 MPa vs. 273.8 ± 41.5 MPa; depressed displacement: 0.123 ± 0.036 mm vs. 0.133 ± 0.049 mm vs. 0.158 ± 0.050 mm; separated displacement: 0.402 ± 0.031 mm VS 0.412 ± 0.047 mm VS 0.437 ± 0.049 mm). The larger the offset of the support position was, the larger the peak screw stress and the larger the reduction loss of depressed and separated fragment reduction, regardless of the support size. The medium support combined with the central position presented the minimum of peak stress and reduction loss. Cortical bone was below 2 % and trabecular strain was below 10 % for all scenarios.
Conclusion: Central placement of structural support provides superior stability for the treatment of depressed tibial plateau fractures compared to the eccentric placement. When a support is placed centrally, optimal stability is achieved when the diameter matches the diameter of the depressed region. Thus, the utilization of equal-diameter fillers to provide central support appears to be an ideal selection for depressed tibial plateau fractures.

1. Introduction

Tibial plateau fractures (TPFs) account for 1 % of all fractures, whereas depressed TPFs account for a significant 50.2 % of TPFs [1],

* Corresponding author.
E-mail address: bszw@hotmail.com (W. Zhang).
[1] These authors contributed equally to this work and should be considered co-first authors.

https://doi.org/10.1016/j.heliyon.2024.e29453
Received 15 June 2023; Received in revised form 7 April 2024; Accepted 8 April 2024
Available online 10 April 2024

an injury type which has not yet been included in AO/OTA 41-C2/3 types. The general treatment principle for this type of fracture is anatomic reduction and rigid fixation for primary healing [2]. However, due to its specific fracture morphology and inconsistent treatment, satisfactory outcomes have not been achieved in the treatment of TPFs. The incidences of osteoarthritis (OA) after TPFs varies in the literature between 10 % and 58 % [3].

Failure to achieve and maintain reduction and maintenance of the depressed fragment is one of the most important factors in rapid knee degeneration, which increases the likelihood of requiring total knee replacement approximately one year after surgery [4–6]. According to the treatment guidelines of the AO group, Cancellous granule graft is needed after depressed fragment reduction, but long-term clinical follow-up has shown that the granular bone grafts does not seem to achieve satisfactory effects [7].

In recent years, the structural-support approach has been extensively studied. In a study conducted by Li et al. [8], 18 patients with depressed TPFs were treated with titanium mesh + allograft as an adjunct to open reduction internal fixation (ORIF), and no significant changes in the step-off values of the articular surface, joint mobility, or posterior tibial angle were found during the 1-year radiological follow-up. This suggested that structural support may be a potentially effective adjunctive treatment modality. Additionally, the structural bicortical iliac treatment conducted by Wang et al. exhibited favorable radiological follow-up results [9]. We subsequently conducted mechanical tests of the structural-support approach, and finite element analysis results showed that it significantly reduced the risk of secondary subsidence of the articular surface compared to granular support when the screws were able to penetrate the depressed fragment or filler [10]. The above studies affirm the good mechanical benefits of providing structural support for depressed TPFs, but the effect of the position and size of different structural supports on the stability of these fractures remains to be investigated.

The aim of this work was to investigate the effect of the position and size of different structural supports on the stability of depressed TPFs and to provide a reference for the practice of structural support strategies in clinical practice.

2. Materials and methods

2.1. Geometry of tibial plateau fracture

The tibial plateau utilized in this work was generated from computed tomography scans of the knee of a healthy female volunteer, aged 65, with a weight of 75 kg. The patient was fully informed regarding the use of the data in advance and provided written informed consent. A Siemens AG 64-slice CT scanner from Germany was used to acquire CT scans with a slice thickness of 1.0 mm. The acquired data were subsequently imported into Mimics (Materialize, Belgium). A semi-automatic segmentation technique utilizing the region growing algorithm was applied to produce three-dimensional models of both cortical and cancellous bone. Following this, the initial model underwent smoothing and processing using Geomagic Wrap software from 3D Systems in the United States. Ultimately, the modified geometries were transferred into NX Unigraphics, a software developed by Siemens PLM based in the United States, to execute geometric shape division, facilitating the creation of the fracture line.

The split-depressed tibial plateau fracture mode employed in this study was adapted from Yao et al. 's fracture map of tibial plateau [11]. This model comprised four components: the bone shaft, depressed fragment, separated fragment, and coloboma site. The depressed fragment was modeled as a cylinder, with a diameter of 14 mm and a height of 10.5 mm, which was positioned with the inferior edge of the split fracture line approximately 3.5 cm from the articular surface. The defect area was set with a diameter of 14

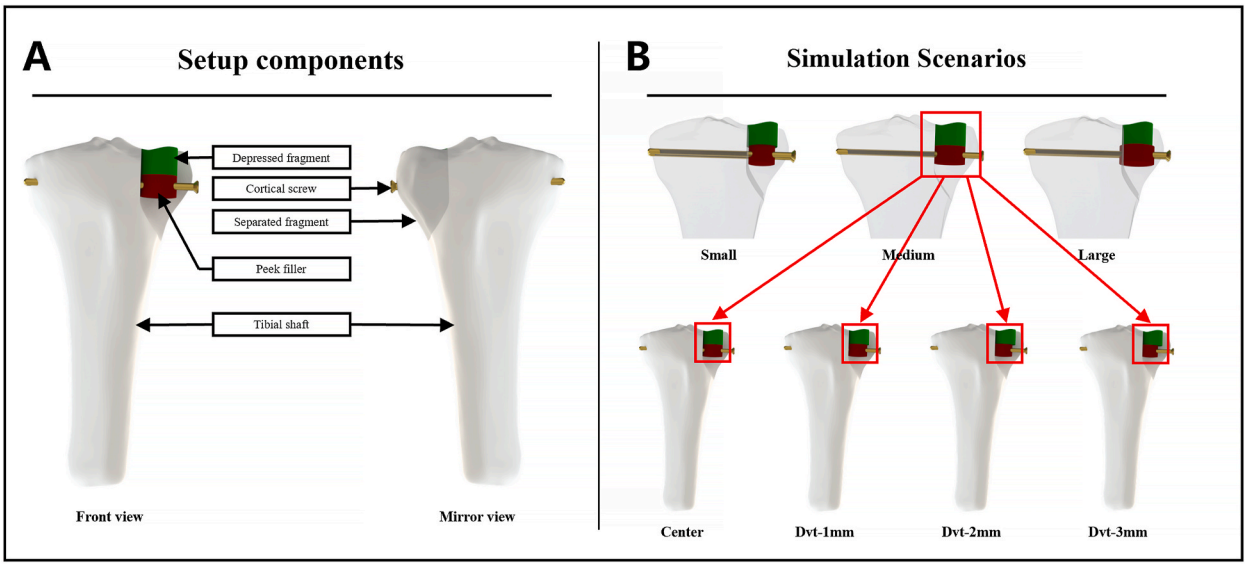

Fig. 1. (A): Frontal view of the setup showed the components including: depressed fragment, Peek filler, cortical screw and tibial shaft, and the mirror view showed the separated fragment. (B): The top three diagrams showed three simulated filler sizes, each differing by 2 mm. The four diagrams below showed the four locations of each filler, deviating 3 mm from center to inside.

mm and a height of 10 mm. For fracture stabilization, we employed two cortical screws with a diameter of 3.5 mm, sourced from AKEC in China, following the method outlined in the Bansal study [12]. Although acknowledging some deviation from reality, the screw was assumed to have no screw threads for geometrical simplification, aiming to enhance simulation processing time. The setup components were detail described in Fig. 1A. The simulation scenarios were divided into three groups with different structural filler diameters of 12 mm, 14 mm, and 16 mm to investigate the mechanical response to fillers of different sizes. Each group of models included four working conditions: central filler placement and filler placement offset 1 mm, 2 mm, and 3 mm inwards (Fig. 1B), to investigate the influence of support position on stability. A total of 12 simulation scenarios were included for the three sizes combined with the four positions.

2.2. Material properties of each structure

The 12 profiles were imported into Hypermesh (Altair; United States) for meshing and material property assignment. Meshing of the model's diverse components was accomplished using tetrahedral elements, following the methodology advocated in the literature [13]. To achieve a refined mesh, a series of simulations were performed by incrementally adjusting the degree of refinement until the maximum displacement values stabilized within a 5 % variation. The resultant meshes consisted of tetrahedral elements, with an average size of 1.42 mm, in accordance with the guidelines established by Burkhart et al. regarding angle idealization, aspect ratio and Jacobian element for tetrahedral elements [14] (Fig. 2B). The total counts of elements and nodes for the entire working conditions are detailed in Table 1.

Homogeneous orthotropic linear elastic material models were assumed for bone structures [15], whereas screw models were assigned homogeneous isotropic linear elastic material models. The filler was set as 3D printed PEEK with an elastic modulus of 2.8 GPa [16], and the screw properties were set as titanium alloy with an elastic modulus of 110 GPa [15], both of which are clinically common material. The density of all materials was established according to Guneri et al. 's description [17]. Detailed properties of all materials were shown in Table 2.

2.3. Boundary conditions

Abaqus/CAE (Dassault Systems, United States) was utilized for defining boundary conditions and conducting simulations. As was described by Taylor et al. the loading conditions were selected to mimic a scenario where the patient experiences single-leg stance, which equated to three times the body weight [18]. As a consequence, there was a cumulative force of 2250 N, allocated between the medial (1417.5 N) and lateral condyles (832.5 N) [19] (Fig. 2A). The resultant contact surfaces approximately measured 403 mm^2 for the lateral condyles and 374 mm^2 for the medial condyles [20]. The lower surface of the tibia model was constrained to exhibit zero displacement across all degrees of freedom.

It was assumed that the screws and bone was fully fixed, the interface between two components was considered perfectly bonded.

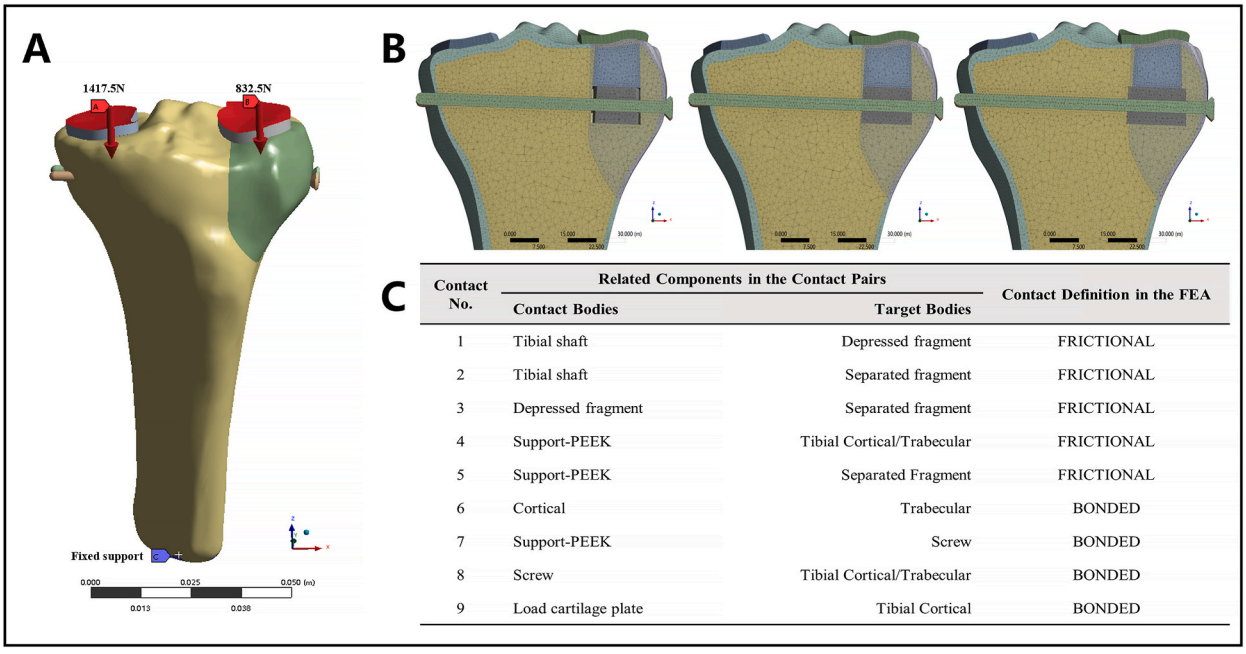

Contact No.	Related Components in the Contact Pairs		Contact Definition in the FEA
	Contact Bodies	Target Bodies	
1	Tibial shaft	Depressed fragment	FRICTIONAL
2	Tibial shaft	Separated fragment	FRICTIONAL
3	Depressed fragment	Separated fragment	FRICTIONAL
4	Support-PEEK	Tibial Cortical/Trabecular	FRICTIONAL
5	Support-PEEK	Separated Fragment	FRICTIONAL
6	Cortical	Trabecular	BONDED
7	Support-PEEK	Screw	BONDED
8	Screw	Tibial Cortical/Trabecular	BONDED
9	Load cartilage plate	Tibial Cortical	BONDED

Fig. 2. (A): Bounding condition of the models during loading. The medial and lateral condyles were loaded at 1417.5 N and 832.5 N, respectively, while the distal tibia was fixed. (B): From left to right, mesh details from small to large. (C): Component contact relationships List.

Table 1
The number of nodes and elements for the whole models.

Nodes/Elements	Group A	Group B	Group C
Tibial shaft	478944 ± 842/90099 ± 113	478801 ± 564/90117 ± 114	477033 ± 687/89856 ± 94
Depressed fragment	51178/10578	51178/10418	51178/10418
Separated fragment	58613 ± 7789/12700 ± 2110	57566 ± 6425/13597 ± 3252	57713 ± 7979/12522 ± 2153
Support	10889 ± 393/2418 ± 70	12942 ± 311/2858 ± 56	16235 ± 155/3537 ± 23
Screw	17809/4582	17809/4582	17809/4582
Total	617433 ± 9024/120377 ± 2293	618296 ± 7300/121572 ± 3422	619968 ± 8821/120915 ± 2270

Table 2
Material properties assigned in the FEA setup.

Model Components	Young modulus (MPa)	Poisson's ratio	Density (kg m^{-3})
Cortical bone	$E_3 = 12847$	$\upsilon_{12} = 0.381$	1980
	$E_2 = 7098$	$\upsilon_{13} = 0.172$	
	$E_1 = 6498$	$\upsilon_{23} = 0.167$	
	$G_{12} = 2290$	$\upsilon_{21} = 0.396$	
	$G_{13} = 2826$	$\upsilon_{31} = 0.376$	
	$G_{23} = 3176$	$\upsilon_{32} = 3.346$	
Trabecular bone	$E_3 = 370.6$	$\upsilon_{12} = 0.381$	
	$E_2 = 123.4$	$\upsilon_{13} = 0.104$	
	$E_1 = 123.4$	$\upsilon_{23} = 0.104$	
	$G_{12} = 44.84$	$\upsilon_{21} = 0.381$	830
	$G_{13} = 58.18$	$\upsilon_{31} = 0.312$	
	$G_{23} = 58.18$	$\upsilon_{32} = 0.312$	
Titanium alloy screw	E = 110000	$\upsilon = 0.3$	4500
PEEK	E = 2800	$\upsilon = 0.3$	1350

Additionally, accounting for the fluid microenvironment surrounding the fragment post-surgery, the surfaces between the fragments and between the bone and the support were defined to have frictional contact and the friction coefficient was defined as 0.2 [21]. As the support is typically implanted by tamping technique in actual clinical scenarios [22], the lower surface of the filler is not supported by the bone. For this reason, we did not set the contact relationship between the lower surface of the support and the underlying bone to match the real surgical scenario. Detailed information regarding the contact between components was presented in Fig. 2C.

3. Results

Stress, strain, and displacement fields were recorded to assess the likelihood of implant failure and the potential for loss of fragment reduction. Specifically, the stress field of the screw was analyzed to identify areas of potential weakness. Reduction loss was quantified by examining the axial displacement for the depressed fragment and the degree of separation of the separate fragment in the medial-

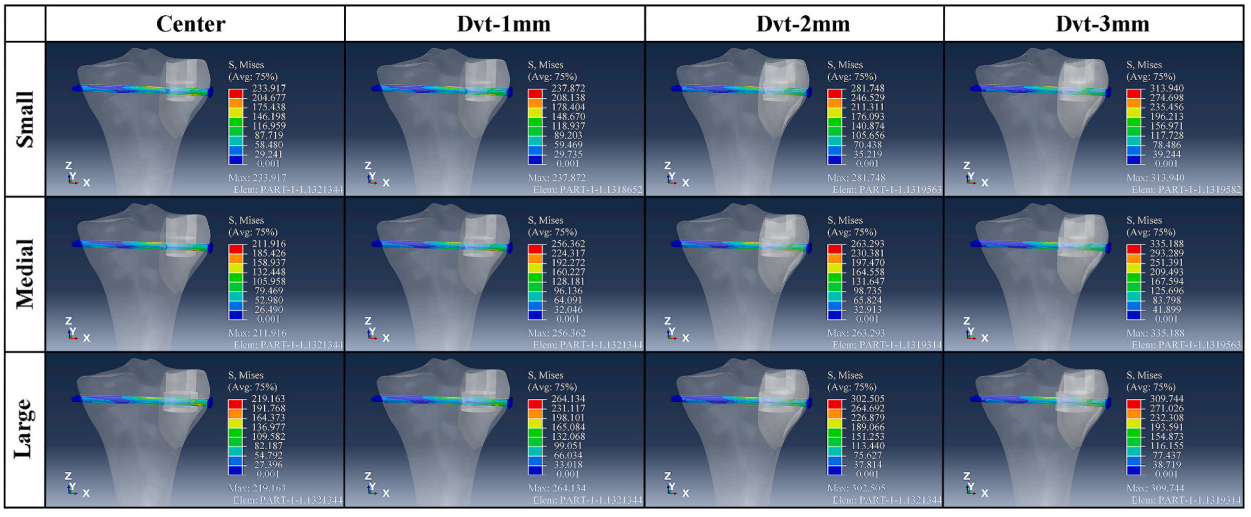

Fig. 3. Von-Mises stress (MPa) distribution of the screws under 12 simulated scenarios. The legend shows the maximum stress for each condition, with all peaks located in the same region.

lateral direction.

The stress distribution field of the screw was presented in Figs. 3 and 7-A for the twelve scenarios. The peak stress of the screw stress in all scenarios was at the lateral edge where the screw intersects the filler. Regardless of the size of the support, the minimum peak stress of the screw was obtained with central placement compared to eccentric placement. In the small support group, the peak screw stress was 233.9, 237.9, 281.7 and 313.0 MPa when the placement was changed from the center to the deviation by 3 mm, respectively. In the medium support group, the peak screw stress was 211.9, 256.4, 263.3 and 335.2 MPa, respectively, and in the large support group, it was 219.2, 264.1, 302.5, 309.7 M. When all three sizes of supports were placed in the central position, the medium-sized support group seemed to exhibit the smallest screw stress concentration; the screw stress in eccentric placement did not show significant regularity, but the peak stress were within the yield strength range in all scenarios.

The opening displacement field of the separated fragment was presented in Figs. 4 and 7-B for all scenarios. The separated fragment displacement exhibited the same trend as the peak screw stress. The displacement corresponding to 3 mm offset from the center was 0.089, 0.096, 0.146, and 0.162 mm, respectively, in the small support group; 0.077, 0.108, 0.159, and 0.188 mm in the medium support group; 0.108, 0.123, 0.187, and 0.214 mm in the large support group. For the central support, the medium-sized support exhibited the minimum separated displacement; however, in all cases with different degrees of deviation, the small support exhibited the minimum reduction loss.

The axial displacement field of the depressed fragment was presented in Figs. 5 and 7-C. The displacements were 0.372, 0.383, 0.413, and 0.441 mm in the small support group, 0.360, 0.389, 0.432, and 0.468 mm in the medium support group, and 0.387, 0.409, 0.459, and 0.496 mm in the large support group. Medium support in the central scenario likewise exhibited minimal reduction loss. The small support likewise exhibited minimal axial reduction loss for the scenarios with varying degrees of support deviation, which was consistent with the trend for separated fragment displacement.

In all scenarios, the stress of cortical and cancellous did not exceed the respective yield strength. The strain in cortical was within 2 % in all scenarios, and the maximum strain in cancellous, which was located at the contact site between the screw and the tibial stem, did not exceed 10 % in any of the scenarios, as shown in Fig. 6. According to Perren's strain theory, 2 % and 10 % correspond to the fracture strain of cortical and cancellous [23]. Thus, none of the simulated scenarios exhibited theoretical failure. Nevertheless, an increase in the degree of deviation appeared to raise the risk of failure.

4. Discussion

4.1. Lag screw fixation

Raft plate and screw technique, as a popular fixation method in recent years, has been proven by biomechanical studies to provide the best axial compression resistance and is especially suitable for osteoporotic TPFs and depressed TPFs with comminuted articular surface [24].

For simple fractures of the articular surface, many scholars recommend the use of 6.5 mm or 3.5 mm lag screws for percutaneous fixation, which can compress the fracture fragments with minimal damage to the surrounding soft tissue. Although the lag screw technique does not provide the same compression resistance as the raft plate screw technique, the two fixation methods have the same effect on maintaining position for 6 weeks of non-weight-bearing exercise [25]. In addition, the percutaneous screw technique causes

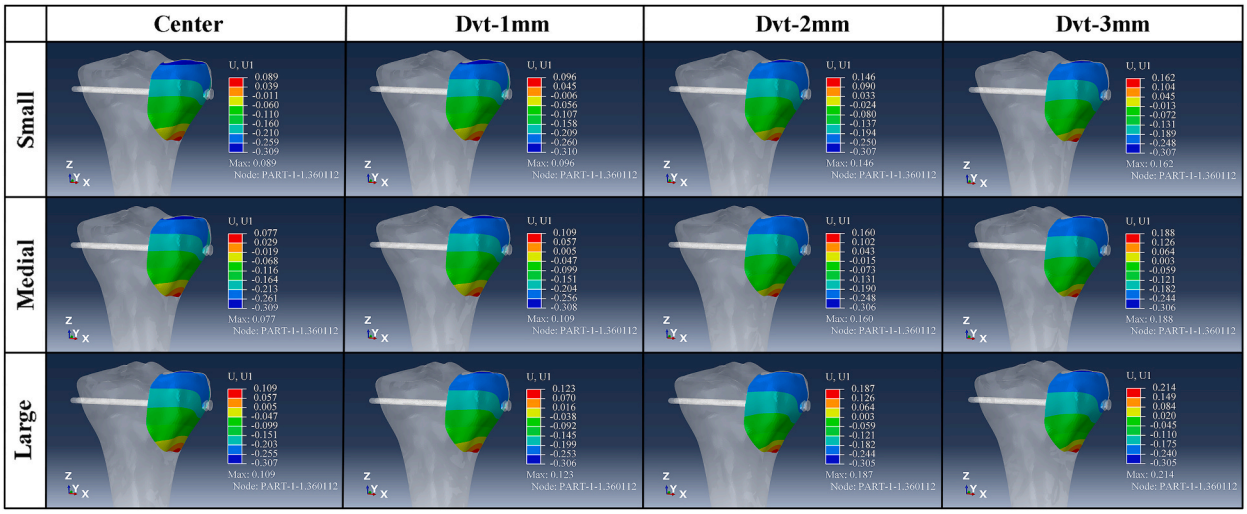

Fig. 4. Directional displacement (mm) distribution field of the Separated fragment under 12 simulated scenarios. U1 represents the positive direction of the X-axis of the coordinate system, and negative X-axis displacement of separated fragment was used to indicate the extent of reduction loss.

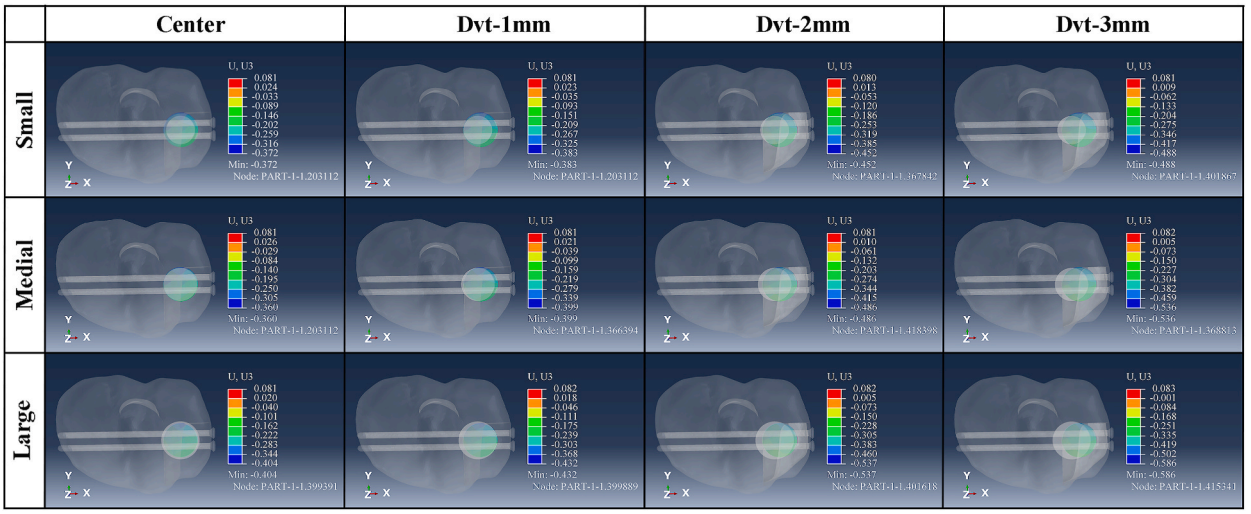

Fig. 5. Axial displacement (mm) distribution field of the depressed fragment under 12 simulated scenarios. U3 represents the positive direction of the Z-axis of the coordinate system, and negative Z-axis displacement of depressed fragment was used to indicate the extent of reduction loss.

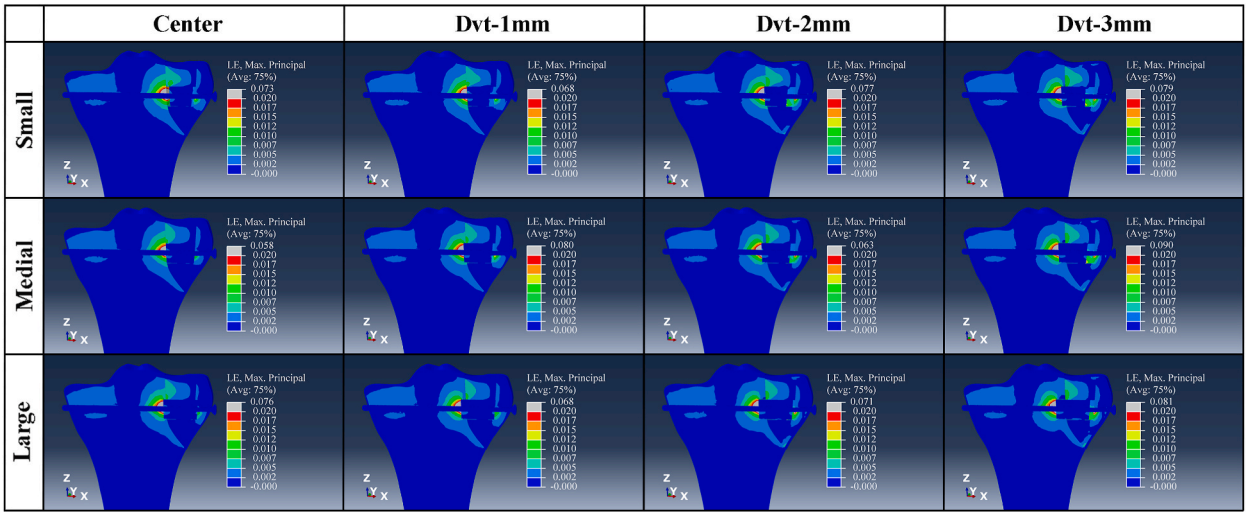

Fig. 6. Typical cross section of strain field in all scenarios. The maximum strain occurred in the area of the cancellous in contact with the filler. The strain of the cancellous did not exceed 10 % in any of the scenarios.

the minimum damage of the muscle and ligament with maximum preservation of the original supporting structure of the knee joint, which can not only avoid the irritation caused by internal fixation, but also provide an anatomical basis for complete functional recovery.

4.2. Structural support

The management of epiphyseal defects is still controversial. Autologous bone graft, considered the gold standard due to its superior biological properties, has been challenged by scholars exploring alternative bone substitute materials in light of the complications associated with bone harvesting surgery [26]. The current options for bone graft substitutes can be categorized into two types: granular and structural. Autologous or allogeneic bone particles represent the former [12,27,28], while bone cement and bioactive materials are examples of the latter [9,29–31]. Long-term clinical follow-up results have shown that the incidence of secondary depression of the articular surface is less with the latter than the former [7], which may be attributed to the good mechanical properties these materials possess.

Exactly how the mechanical performance of different structural support methods ultimately affects stability is an interesting topic. We previously performed multiple finite element simulations with raft-plate combined with structural support techniques and found that structural support with minimal stiffness resulted in a significantly reduced risk of fixation failure compared to granular supports

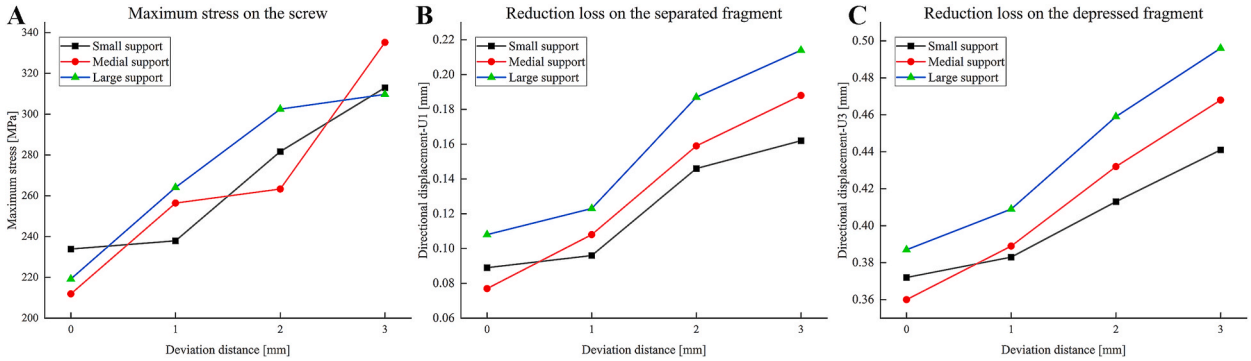

Fig. 7. (A): For each size of the support, the peak stress of the screw increases with the deviation of the filler. (B): Displacements in the medial-lateral direction (U1) were used to represent the reduction loss of the separated fragment, which increased with the deviation distance of the filler. (C): Displacements in the axial direction (U3) were used to represent the reduction loss of the depressed fragment, which showed the same trend as the separated fragment. Whether it is screw stress or fragment reduction loss, the center-positioned medial support provides optimal mechanical performance.

when screws were passed through or braced depressed bone [10], which was consistent with the findings of a cadaveric bone biomechanics study by Benoit et al. [32]. However, the stiffness of the filler when screws were held against the filler had a greater impact. Screw anchors filler is a very common clinical scenario, for example, the use of lag screws can be threaded through the bicortical iliac graft for effective structural support after reduction of the depressed fragment and implantation by the tamping technique [9]. The same principle is used in tuberoplasty, where a pressure balloon is used to compact the surrounding cancellous, which in turn is injected with polymethyl methacrylate (PMMA) cement, and finally screws are threaded through the unconsolidated bone cement for support [32]. Bone cement has a stiffness of approximately 2–3 GPa and has demonstrated good radiographic and functional outcomes in multiple clinical follow-up studies [33,34]. However, tuberoplasty has two potential technical drawbacks: the pressure of the balloon does not allow for true reduction, and the top pressure of the balloon on the surrounding bone does not achieve the effect of conventional tamping, thus reducing the stability between the fracture fragments.

Therefore, we tested a structural filler with similar stiffness to bone cement with the ability to compensate for both of these deficiencies, i.e. 3D printed PEEK. As a more reliable structural support that could be implanted into the defect by tamping, which was the origin of our experimental design using PEEK.

4.3. Support size and position

The small structural support corresponds to the bicortical iliac or fibula grafts. Due to the limitation of the bone harvesting area, autologous iliac and fibula grafts can be obtained in most cases as long strip-like structures with small diameters [35], which cannot be fully covered, as shown in Fig. 8A. The medium and large supports correspond to bone cement in clinical scenarios. Due to the differences in fracture morphology and reduction techniques, it is easier to obtain a support area with a diameter similar to the depressed area by balloon reduction tuberoplasty, but the diameter of the bone cement support implanted after reduction by window tamping technique is significantly larger than the size of the depressed bone [36,37], as shown in Fig. 8B and C. Furthermore, regardless of the reduction method, differences in proficiency between surgical operators led to differences in the precision of reduction and the placement of the filler, as shown in Fig. 8B, where the cement support is not located directly below the depressed area. As two realistic clinical problems, the ultimate effect of support size and position on stability is not known, thus, we conducted this study.

As shown in Fig. 7A–C, the peak stress on the screw, the reduction loss of both the separated and depressed fragments exhibited a consistent upward trend as the deviation increased, regardless of the size of the support, indicating that the position of the support is indeed an important variable affecting stability. Additionally, the medium-sized support exhibited the minimum loss of depressed fragment reduction in the central position. Under similar deviation conditions, the small support demonstrated the least reduction loss, while displacement values gradually rose with increasing support. The loss of separated fragment reduction exhibited a pattern consistent with that of the depressed fragment in scenarios with the same degree of offset. However, the peak screw screws did not show a regular pattern.

In our study, small, medium, and large fillers were set as the same material, and the difference in sizes resulted in a difference in mass, while larger diameters produced a larger force arm. The increase in mass and force arm resulted in an increase in the overall resultant moment of the support. Under our boundary conditions, a larger filler size resulted in increased bone destruction and decreased support of the underlying bone, leading to greater reduction loss. However, why did the small size not exhibit minimal loss of axial repositioning under central type placement? We do not think that such a result is contrary to the above principle. Based on the above mode of action, the centrally placed small support created a circular "bare zone" on the lower surface of the depressed bone, which was not supported below. The inner side of the annular zone was deformed more by the axial load on the articular surface, so that this scenario resulted in larger reduction loss of the depressed fragment than in the medium size.

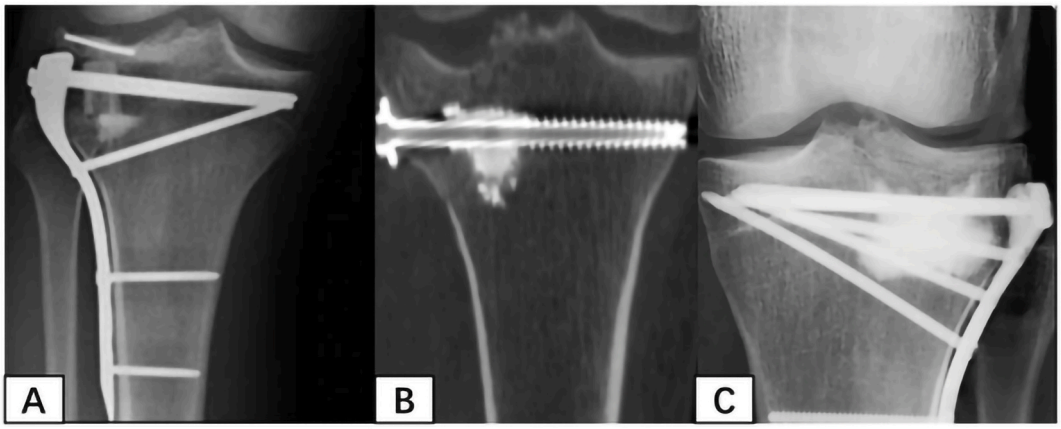

Fig. 8. (A): Small bicortical iliac structural support. (B): Medium-sized cement structural support. (C): Large cement structural support.

4.4. Surgical techniques

Bone grafting through the fracture line or cortical window is the primary means of reducing and maintaining depressed components in the surgical treatment of depressed TPFs. Although autogenous bone has been recognized as the gold standard for bone grafting, bone harvesting does significantly increase the duration of surgery and complications, and its long-term clinical benefit is not satisfactory [26]. Tuberoplasty is performed by ballooning the depressed fragment, but it may not be easily achieved for comminuted or severely depressed articular components [38]. The technique of tamping the depressed components through a fracture line or cortical window under direct visualization followed by implantation of a structural bicortical iliac or fibula is now increasingly used by clinicians [9,35].

The main difference between structural 3D-printed bone substitute materials and the aforementioned approaches is the prospect of their application for all-in-one reduction and implant manipulation by means of a holding device. This is inspired by the working principle of interbody cage in spinal fusion [39], where the holder can act as a reliable bone tamper for defect site tamping, while the support is placed directly in the defect site findings of our present experiment serve as a guide for surgical selection of filler size and placement. The selected filler should correspond to the diameter of depressed fragment and be positioned as centrally as possible below the depressed.

4.5. Validation and limitations

In this study, the effect of the position and size of structural support on the stability of the structure was explored using finite element analysis. As a series of simulation studies, we strictly followed the principle of controlled variables, changing only one variable to study the change in trends within the group. Such a series study ultimately yields a realistic trend result, but if used as individual evidence, the values are needed for cadaver bone validation experiments. The calculated results of individual scenarios are not referable without biomechanical experimental validation, but the serial comparison eliminates the computational bias due to errors in the simulation parameters and yields a relatively realistic and credible trend of variation instead. In addition, the stress distribution of bone we derived is similar to that obtained by Aubert et al. [40] and Belaid et al. [15], which indirectly proves the rationality of our model.

As a bone simulation study, assigning material properties based on the true density variance-HU (Hounsfield unit) of bone is the most realistic and reliable approach. It reflects the true bearing loads inside the bone and pinpoints the location of peak stress/strain. Considering the convenience of model geometry setting in this study, the direct assignment of Young's modulus is used to define the material properties of bone. It is undeniable that the method of assigning material properties based on HU values will significantly increase the reliability of the results under each simulated condition, and thus significantly increase the reliability of the overall study results and conclusions.

Certainly, there are some limitations to this study. Soft tissue structures such as ligaments, meniscus, and muscles were not included in the simulation, and the contact relationships between the components were based on a limited reference [15,21], mainly because there is no clear consensus on these parameters. We used only a single axial compressive load, which only reflects the stability of the structure under the maximum axial compressive load. The shear load under flexion and extension is equally important, but this requires the definition of more stringent and validated boundary conditions, for which no relevant studies have been reported. In addition to the above deficiencies, the lack of testing for fatigue under cyclic loading is one shortcoming of this work. Further studies should perform validation experiments of the same design on a cadaveric knee joint.

5. Conclusion

The central placement of the structural support provides superior stability for the treatment of depressed TPFs compared to the eccentric placement. When a support is placed centrally, optimal stability is achieved when the diameter of the support matches the diameter of the depressed region. Thus, the utilization of equal-diameter fillers to provide central support appears to be an ideal selection for depressed tibial plateau fractures.

Ethics and consent

This study was approved by the Ethics Committee of PLA General Hospital (S2020-114-01). The participant had signed the written informed consent and agreed to participate in this study and have their information published.

Funding statement

This research was supported by NO. 2021-NCRC-CXJJ-ZH-25 of Clinical Application-oriented Medical Innovation Foundation from National Clinical Research Center for Orthopedics, Sports Medicine & Rehabilitation Foundation, and the National Natural Science Foundation of China (82172451). The funders had no role in the study design, data collection and analysis, decision to publish, or preparation of the manuscript.

Data availability statement

Data included in article/supp. material/reference in article.

CRediT authorship contribution statement

Xiaomeng Ren: Writing – original draft, Visualization, Investigation, Formal analysis. **Cheng Xu:** Validation, Software, Methodology. **Yu Jiang:** Supervision, Resources, Formal analysis, Data curation. **Da Teng:** Project administration, Methodology, Investigation. **Xinmo Liu:** Supervision, Project administration, Data curation. **Junsong Wang:** Funding acquisition, Formal analysis, Data curation, Conceptualization. **Wei Zhang:** Writing – review & editing, Supervision, Funding acquisition, Conceptualization.

Declaration of competing interest

The authors declare that they have no competing financial interests or personal relationships that could have appeared to influence the work reported in this paper.

References

[1] R. Elsoe, P. Larsen, N.P. Nielsen, J. Swenne, S. Rasmussen, S.E. Ostgaard, Population-based epidemiology of tibial plateau fractures, Orthopedics 38 (9) (2015 Sep) e780–e786, https://doi.org/10.3928/01477447-20150902-55.
[2] M.K. Júnior, F. Fogagnolo, R.C. Bitar, R.L. Freitas, R. Salim, C.A. Jansen Paccola, tibial plateau fractures, Rev Bras Ortop. 44 (6) (2015 Dec 7) 468–474, https://doi.org/10.1016/S2255-4971(15)30142-7.
[3] M.V. Rademakers, G.M. Kerkhoffs, I.N. Sierevelt, E.L. Raaymakers, R.K. Marti, Operative treatment of 109 tibial plateau fractures: five- to 27-year follow-up results, J. Orthop. Trauma 21 (1) (2007 Jan) 5–10, https://doi.org/10.1097/BOT.0b013e31802c5b51.
[4] P.F. Lachiewicz, T. Funcik, Factors influencing the results of open reduction and internal fixation of tibial plateau fractures, Clin. Orthop. Relat. Res. 259 (1990 Oct) 210–215.
[5] S. Parratte, M. Ollivier, J.N. Argenson, Primary total knee arthroplasty for acute fracture around the knee, Orthop Traumatol Surg Res 104 (1S) (2018 Feb) S71–S80, https://doi.org/10.1016/j.otsr.2017.05.029.
[6] E.P. Su, G.H. Westrich, A.J. Rana, K. Kapoor, D.L. Helfet, Operative treatment of tibial plateau fractures in patients older than 55 years, Clin. Orthop. Relat. Res. 421 (2004 Apr) 240–248, https://doi.org/10.1097/01.blo.0000119247.60317.bc.
[7] T. Goff, N.K. Kanakaris, P.V. Giannoudis, Use of bone graft substitutes in the management of tibial plateau fractures, Injury 44 (Suppl 1) (2013 Jan) S86–S94, https://doi.org/10.1016/S0020-1383(13)70019-6.
[8] J. Li, Z. Li, M. Wang, H. Zhang, Y. Liang, W. Zhang, Fixation augmentation using titanium cage packing with xenograft in the treatment of tibial plateau fractures, Injury 51 (2) (2020 Feb) 490–496, https://doi.org/10.1016/j.injury.2019.10.025.
[9] Z. Wang, Y. Zhu, X. Deng, Xin Xing, S. Tian, L. Fu, X. Yan, W. Chen, Z. Hou, Y. Zhang, Structural bicortical autologous iliac crest bone graft combined with the tunnel bone tamping method for the depressed tibial plateau fractures, BioMed Res. Int. 2021 (24) (2021 Aug) 1249734, https://doi.org/10.1155/2021/1249734.
[10] C. Zeng, X. Ren, C. Xu, M. Hu, J. Li, W. Zhang, Stability of internal fixation systems based on different subtypes of Schatzker II fracture of the tibial plateau: a finite element analysis, Front. Bioeng. Biotechnol. 10 (2022 Sep 7) 973389, https://doi.org/10.3389/fbioe.2022.973389.
[11] X. Yao, K. Zhou, B. Lv, L. Wang, J. Xie, X. Fu, J. Yuan, Y. Zhang, 3D mapping and classification of tibial plateau fractures, Bone Joint Res 9 (6) (2020 Jul 23) 258–267, https://doi.org/10.1302/2046-3758.96.
[12] M.R. Bansal, S.B. Bhagat, D.D. Shukla, Bovine cancellous xenograft in the treatment of tibial plateau fractures in elderly patients, Int. Orthop. 33 (3) (2009 Jun) 779–784, https://doi.org/10.1007/s00264-008-0526-y.
[13] K. Polgar, M. Viceconti, J.J. O'Connor, A comparison between automatically generated linear and parabolic tetrahedra when used to mesh a human femur, Proc. Inst. Mech. Eng. H 215 (1) (2001) 85–94, https://doi.org/10.1243/0954411011533562.
[14] T.A. Burkhart, D.M. Andrews, C.E. Dunning, Finite element modeling mesh quality, energy balance and validation methods: a review with recommendations associated with the modeling of bone tissue, J. Biomech. 46 (9) (2013 May 31) 1477–1488, https://doi.org/10.1016/j.jbiomech.2013.03.022.
[15] D. Belaid, T. Vendeuvre, A. Bouchoucha, F. Brémand, C. Brèque, P. Rigoard, A. Germaneau, Utility of cement injection to stabilize split-depression tibial plateau fracture by minimally invasive methods: a finite element analysis, Clin. Biomech. 56 (2018 Jul) 27–35, https://doi.org/10.1016/j.clinbiomech.2018.05.002.

[16] J. Kang, J. Zhang, J. Zheng, L. Wang, D. Li, S. Liu, 3D-printed PEEK implant for mandibular defects repair-a new method, J. Mech. Behav. Biomed. Mater. 116 (2021 Apr) 104335, https://doi.org/10.1016/j.jmbbm.2021.104335.
[17] B. Guneri, O. Kose, H.K. Celik, A. Cakar, E. Tasatan, A.E.W. Rennie, How to fix a tibial tubercle osteotomy with distalisation: a finite element analysis, Knee 37 (2022 Aug) 132–142, https://doi.org/10.1016/j.knee.2022.06.002.
[18] W.R. Taylor, M.O. Heller, G. Bergmann, G.N. Duda, Tibio-femoral loading during human gait and stair climbing, J. Orthop. Res. 22 (3) (2004 May) 625–632, https://doi.org/10.1016/j.orthres.2003.09.003.
[19] D. Zhao, S.A. Banks, K.H. Mitchell, D.D. D'Lima, C.W. Colwell Jr., B.J. Fregly, Correlation between the knee adduction torque and medial contact force for a variety of gait patterns, J. Orthop. Res. 25 (6) (2007 Jun) 789–797, https://doi.org/10.1002/jor.20379.
[20] S.Y. Poh, K.S. Yew, P.L. Wong, S.B. Koh, S.L. Chia, S. Fook-Chong, T.S. Howe, Role of the anterior intermeniscal ligament in tibiofemoral contact mechanics during axial joint loading, Knee 19 (2) (2012 Mar) 135–139, https://doi.org/10.1016/j.knee.2010.12.008.
[21] U. Simon, P. Augat, A. Ignatius, L. Claes, Influence of the stiffness of bone defect implants on the mechanical conditions at the interface–a finite element analysis with contact, J. Biomech. 36 (8) (2003 Aug) 1079–1086, https://doi.org/10.1016/s0021-9290(03)00114-3.
[22] Y. Liu, Z. Liao, L. Shang, W. Huang, D. Zhang, G. Pei, Characteristics of unilateral tibial plateau fractures among adult patients hospitalized at an orthopaedic trauma centre in China, Sci. Rep. 7 (2017 Jan 11) 40647, https://doi.org/10.1038/srep40647.
[23] S.M. Perren, Evolution of the internal fixation of long bone fractures. The scientific basis of biological internal fixation: choosing a new balance between stability and biology, J Bone Joint Surg Br 84 (8) (2002 Nov) 1093–1110, https://doi.org/10.1302/0301-620x.84b8.13752.
[24] WW 3rd Cross, B.A. Levy, J.A. Morgan, B.M. Armitage, P.A. Cole, Periarticular raft constructs and fracture stability in split-depression tibial plateau fractures, Injury 44 (6) (2013 Jun) 796–801, https://doi.org/10.1016/j.injury.2012.12.028.
[25] J.B. Arnold, C.G. Tu, T.M. Phan, M. Rickman, V.D. Varghese, D. Thewlis, L.B. Solomon, Characteristics of postoperative weight bearing and management protocols for tibial plateau fractures: findings from a scoping review, Injury 48 (12) (2017 Dec) 2634–2642, https://doi.org/10.1016/j.injury.2017.10.040.
[26] C. Myeroff, M. Archdeacon, Autogenous bone graft: donor sites and techniques, J Bone Joint Surg Am 93 (23) (2011 Dec 7) 2227–2236, https://doi.org/10.2106/JBJS.J.01513.
[27] W. Feng, L. Fu, J. Liu, D. Li, X. Qi, The use of deep frozen and irradiated bone allografts in the reconstruction of tibial plateau fractures, Cell Tissue Bank. 14 (3) (2013 Sep) 375–380, https://doi.org/10.1007/s10561-012-9342-0.
[28] N. Lasanianos, G. Mouzopoulos, C. Garnavos, The use of freeze-dried cancelous allograft in the management of impacted tibial plateau fractures, Injury 39 (10) (2008 Oct) 1106–1112, https://doi.org/10.1016/j.injury.2008.04.005.
[29] J.Y. Wang, C.Y. Cheng, A.C. Chen, Y.S. Chan, Arthroscopy-assisted corrective osteotomy, reduction, internal fixation and strut allograft augmentation for tibial plateau malunion or nonunion, J. Clin. Med. 9 (4) (2020 Apr 1) 973, https://doi.org/10.3390/jcm9040973.
[30] T. Rolvien, F. Barvencik, T.O. Klatte, B. Busse, M. Hahn, J.M. Rueger, M. Rupprecht, ß-TCP bone substitutes in tibial plateau depression fractures, Knee 24 (5) (2017 Oct) 1138–1145, https://doi.org/10.1016/j.knee.2017.06.010.
[31] R. Iundusi, E. Gasbarra, M. D'Arienzo, A. Piccioli, U. Tarantino, Augmentation of tibial plateau fractures with an injectable bone substitute: CERAMENT™. Three year follow-up from a prospective study, BMC Muscoskel. Disord. 16 (2015 May 13) 115, https://doi.org/10.1186/s12891-015-0574-6.
[32] B. Benoit, Z. Fouad, G.H. Laflamme, D. Rouleau, G.Y. Laflamme, Augmentation of tibial plateau fractures with Trabecular Metal: a biomechanical study, J. Orthop. Surg. Res. 4 (2009 Sep 22) 37, https://doi.org/10.1186/1749-799X-4-37.
[33] A. Hanke, M. Bäumlein, S. Lang, B. Gueorguiev, M. Nerlich, T. Perren, P. Rillmann, C. Ryf, T. Miclau, M. Loibl, Long-term radiographic appearance of calcium-phosphate synthetic bone grafts after surgical treatment of tibial plateau fractures, Injury 48 (12) (2017 Dec) 2807–2813, https://doi.org/10.1016/j.injury.2017.10.030.
[34] M. Ollivier, M. Turati, M. Munier, A. Lunebourg, J.N. Argenson, S. Parratte, Balloon tibioplasty for reduction of depressed tibial plateau fractures: preliminary radiographic and clinical results, Int. Orthop. 40 (9) (2016 Sep) 1961–1966, https://doi.org/10.1007/s00264-015-3047-5.
[35] M.B. Berkes, M.T. Little, P.C. Schottel, N.C. Pardee, A. Zuiderbaan, L.E. Lazaro, D.L. Helfet, D.G. Lorich, Outcomes of Schatzker II tibial plateau fracture open reduction internal fixation using structural bone allograft, J. Orthop. Trauma 28 (2) (2014 Feb) 97–102, https://doi.org/10.1097/BOT.0b013e31829aaee1.
[36] T. Vendeuvre, V. Ferrière, P. Bouget, M. Billot, A. Germaneau, M. Severyns, M. Roulaud, P. Rigoard, P. Pries, Percutaneous surgery with balloon for tibial plateau fractures, results with a minimum of 5 years of follow-up, Injury 53 (7) (2022 Jul) 2650–2656, https://doi.org/10.1016/j.injury.2022.05.033.
[37] A. Hofmann, S. Gorbulev, T. Guehring, A.P. Schulz, R. Schupfner, M. Raschke, S. Huber-Wagner, P.M. Rommens, CERTiFy Study Group, Autologous iliac bone graft compared with biphasic hydroxyapatite and calcium sulfate cement for the treatment of bone defects in tibial plateau fractures: a prospective, randomized, open-label, multicenter study, J Bone Joint Surg Am 102 (3) (2020 Feb 5) 179–193, https://doi.org/10.2106/JBJS.19.00680.
[38] T. Vendeuvre, D. Babusiaux, C. Brèque, F. Khiami, V. Steiger, J.F. Merienne, M. Scepi, L.E. Gayet, Tuberoplasty: minimally invasive osteosynthesis technique for tibial plateau fractures, Orthop Traumatol Surg Res 99 (4 Suppl) (2013 Jun) S267–S272, https://doi.org/10.1016/j.otsr.2013.03.009.
[39] V. Palepu, J.H. Peck, E.S. Cadel, A.R. Parikh, S.C. Wagner, D.R. Fredericks Jr., M.D. Helgeson, A.E. Dmitriev, Development of an in vitro test method to simulate intra-operative impaction loading on lumbar intervertebral body fusion devices, J. Biomech. 121 (2021 May 24) 110412, https://doi.org/10.1016/j.jbiomech.2021.110412.
[40] K. Aubert, A. Germaneau, M. Rochette, W. Ye, M. Severyns, M. Billot, P. Rigoard, T. Vendeuvre, Development of digital twins to optimize trauma surgery and postoperative management. A case study focusing on tibial plateau fracture, Front. Bioeng. Biotechnol. 9 (2021 Oct 7) 722275, https://doi.org/10.3389/fbioe.2021.722275.